Metal-cluster fission and the liquid-drop model

Winston A. Saunders*
Institut de Physique Expérimentale, Ecole Polytechnique Fédérale de Lausanne, PHB-Ecublens, CH-1015 Lausanne, Switzerland
(Received 26 December 1991)

Measurements of the fission of multiply charged Au clusters are presented and interpreted in the context of the liquid-drop model. A detailed description of the experimental apparatus is given, with particular attention paid to the cluster source, a liquid-metal ion source. It is found that upon excitation by either photons or collisions, doubly charged clusters in the size range $n=12-18$ atoms may either evaporate a neutral atom or undergo fission, with the tendency towards fission increasing as cluster size decreases. Empirically the relative rate for fission is found to depend on z^2/n. This result is shown to be consistent with the liquid-drop model developed for the fission of heavy nuclei [N. Bohr and J. A. Wheeler, Phys. Rev. 57, 426 (1939)]. The fission barrier height, calculated from the Coulomb and surface energies of a deformed, charged metallic droplet, decreases strongly with cluster size, in agreement with the experimental results.

PACS number(s): 36.40.+d, 61.25.Mv, 24.70.+s, 33.80.Eh

I. INTRODUCTION

When a multiply charged cluster is small enough, the destabilizing influence of the Coulomb repulsion is comparable to the stabilizing influence of the interatomic bonding. In that case, given sufficient internal energy, the cluster can decay into two charged cluster fragments, i.e., undergo fission, with high probability. Fission occurs only in multiply charged systems, and the processes underlying it are physically distinct from those underlying evaporation, which is the dominant decay mode of singly charged and neutral clusters. In multiply charged systems, fission and evaporation compete with one another as decay channels.

The study of multiply charged clusters is precipitated by the desire to understand the behavior of condensed matter the dimensions of which are finite at the atomic scale. Of particular interest is the determination of the range of cluster sizes for which concepts normally associated with bulklike behavior, such as metallic screening, surface tension, and collective motion, obtain. For example, it is known that despite the gradual evolution of band structure in clusters [1] and the organization of the electronic levels into quantized orbitals with well-defined energies and finite occupation numbers (i.e., electronic shell structure) [2], the screening [3] of static and dynamic external electric fields is metalliclike down to sizes in the neighborhood of eight atoms, below which size molecular effects dominate [4]. The study of multiply charged metal-cluster fission addresses similar questions about bulklike behavior from a complementary point of view. Namely, the extent to which models incorporating bulklike descriptions of cluster behavior (surface energy, semiclassical Coulomb self-energies, etc.) provide accurate predictions of cluster behavior the clusters may be said to be manifesting bulklike qualities.

Experimental investigation of the stability of multiply charged clusters dates from the work of Sattler *et al.* (Ref. [5]). In that work, the authors presented mass spectra of charged metallic (Pb), ionic (NaI), and van der Waals (Xe) clusters which showed the presence of doubly charged species only above well-defined cluster sizes. They concluded that only if a doubly charged cluster exceeds a "critical size" will it be stable against spontaneous "Coulomb explosion" or fission.

Subsequent experimental work [6–8] on multiply charged van der Waals bound clusters has considerably extended and strengthened these conclusions about the nature of the critical size in those systems. Well-defined critical sizes n_c^{z+} have been observed in the mass spectra of atomic clusters of Ar, Kr, and Xe, as well as in several molecular cluster systems for charge states up to $z=4$. The measured values of the critical sizes are reproducible [5] and are independent of the method of ionization. While the values of the critical sizes vary widely between different substances (depending, ultimately, on the strength of the van der Waals binding), the ratios of the critical sizes $n_c^{4+}:n_c^{3+}:n_c^{2+}$ scale very closely with the squares of the cluster charges, i.e., 16:9:4 [5].

Measurements of the fragmentation channels of multiply charged van der Waals clusters [9] clearly demonstrate that a competition between fission and evaporation channels occurs just above the critical size in triply charged CO_2 clusters. The tendency to fission (relative to evaporation) was found to increase by several orders of magnitude as the critical cluster size is approached from above. This experimental result put the concept of Coulomb fission (or explosion) on firm experimental ground and showed conclusively why the mass spectra of the van der Waals clusters so reliably and reproducibly indicated the value of the critical size.

Theoretical interpretation of critical sizes and the fission of the van der Waals clusters has also received considerable attention. Early models [10] of the critical sizes were based on considerations of the exothermicity of symmetric mass division. Despite their success in fitting the available experimental data, these models neglected the physically important existence of an energy barrier to

fission. Casero, Saenz, and Soler [11] have proposed a liquid-drop model for van der Waals cluster fission which incorporates the effect of localized charges within the van der Waals cluster on the Coulomb contribution to the deformation energy. This model accurately describes the evolution of the fission barriers and the mass distribution of the fission products as a function of the parent cluster size. In particular, the height of the fission barrier is directly related to observable effects in the mass spectra and the more sophisticated fragmentation measurements.

In contrast, mass spectra have proved to be unreliable indicators of the physics underlying the stability and fragmentation of multiply charged metal clusters [12–15]. As shall be revealed throughout the following discussion, this is, at the most basic level, related to the relatively higher strength of the metallic bond (a few eV) in comparison to a van der Waals bond (a few hundredths of an eV). Comparing these energies to the Coulomb energies important here, ca. 1 eV, shows immediately that bonding effects will be relatively more important in the case of the metals than in the case of van der Waals systems.

Interatomic bonding gives rise to an energy barrier to the fission of clusters. The importance of the fission barrier to the observability of small multiply charged metallic clusters was discussed by Delley [16]. The observability of small multiply charged clusters such as Mo_2^{2+} (Ref. [17]) and Au_2^{2+} (Ref. [18]) is related to the existence of an energy barrier over which the multiply charged cluster must pass en route to fission and not to their absolute stability. Models [19] of multiply charged cluster stability taking only the initial- and final-state energetics into account are incapable of explaining the existence of these metastable species in mass spectra. Even for doubly charged dimers [20] a potential barrier of several tenths of an electron volt separates the metastable bound state from the dissociated fragments. The description of the fission-barrier height, however, depends essentially on the molecular behavior of these small systems. It is conceivable, and in fact is the case, that the fission barriers of larger clusters should depend on cluster properties more closely related to bulklike behavior.

Efforts at addressing the fission-barrier height in metal clusters within a model incorporating bulklike assumptions were made by Sugano *et al.* (Refs. [21,22]), who adapted the liquid-drop model of nuclear fission to clusters. They incorporated shell corrections, following nuclear models, into their predictions of the fission barriers for large highly charged Na clusters (e.g., Na_{50}^{4+}). Lipparini and Vituri [23] have since adapted the liquid-drop model to the fission of doubly charged Na clusters. More recently, Garcias *et al.* (Ref. [24]) have calculated the barrier height for the most asymmetric fission decay of charged Na clusters using the jellium model and the local-density approximation. These models share the common prediction that the barrier height varies strongly with the cluster size and that, as the cluster tends to a well-defined critical size (near ten atoms for doubly charged Na clusters), the height of the barrier vanishes. Molecular-dynamics studies [25] have explored the saddle-point dynamics in considerable detail.

The purpose of this paper is twofold: first, to present fragmentation measurements on multiply charged Au clusters and, second, to interpret these experimental results within the framework of the liquid-drop model. In Sec. II the layout of the experimental apparatus is discussed in some detail. Particular attention is paid to the cluster source, a liquid-metal ion source (LMIS). The configuration of the triple quadrupole mass spectrometer is also discussed. In Sec. III fragmentation measurements on multiply charged Au clusters are presented. Fragmentation is induced both by collisions with background gas atoms and by photoabsorption. The results are discussed in terms of the relative rates for fission and evaporation. This comparison proves fruitful for later comparison to the liquid-drop model.

In Sec. IV the application of the liquid-drop model to metallic clusters is discussed from a theoretical standpoint. Previous work is reviewed and summarized for the sake of defining terminology. The model, which is adapted from that for nuclei, is used to predict the fission-barrier heights and their relation to the evaporation energies of the clusters.

The comparison between the liquid-drop model and the experimental results of this paper is discussed in Sec. V. It is shown that the model provides a coherent interpretation of the available data. In particular, the measured relative fission rates are found to be in good qualitative and quantitative agreement with the prediction of the liquid-drop model. The rate is found to depend primarily on the height of the fission barrier. The general application of the model to the fission multiply charged metallic clusters is also discussed.

The electrostatics calculation for the Coulomb self-energy of a deformed conducting liquid droplet is reserved for an appendix. The calculation shows that, apart from a constant factor, the deformation energy of a conducting liquid droplet is the same to leading order as that of a uniformly charged droplet.

II. EXPERIMENTAL METHOD

The multiply charged Au clusters for these measurements are produced by field extraction by a liquid-metal ion source. The polydisperse beam of ions is energy filtered and then enters a tandem triple quadrupole mass spectrometer where the experiments are performed. The mass spectrometer allows the selection of an individual cluster ion size (more properly, a particular mass-to-charge ratio), the fragmentation of the selected ion, and the analysis of the fragmentation products. In this way, detailed investigations of the relative branching ratios between fission and evaporation channels of the clusters are possible.

A. Cluster source

The high efficiency and excellent long-term stability of LMIS's make them well suited to the production and the study of multiply charged metal clusters. An LMIS is basically a field-emission [26] source and is best suited to metals which have a low vapor pressure at their melting point (to avoid discharges to the high-voltage electrodes)

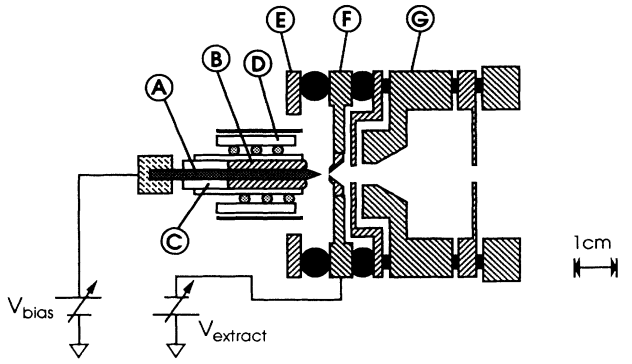

FIG. 1. The liquid-metal ion source (LMIS) used in present experiments. The labeled components are A, the etched tungsten needle; B, molten Au; C, ceramic plug and reservoir; D, heat shield; E, retaining ring; F, high-voltage extractor electrode; and G, asymmetric triode lens system. The connection of the source bias voltage (typically 250–300 V) and the extractor voltage (typically, −5 kV) are shown. Lens supply voltages are not indicated.

and which wet other materials. LMIS's of Au, Ge, Sn, Ga, Si, and the alkali metals have been used in experiments on clusters [27–32].

In comparison with other intense sources of ions (e.g., sputtering) which generate fluxes of neutral particles many orders of magnitude larger than the ion fluxes, LMIS's are highly efficient with regard to material consumption. Most of the material consumed by the LMIS is emitted in the form of ions.

A schematic diagram of the LMIS used in these experiments is shown in Fig. 1. Clusters are emitted from a sharpened tungsten needle which is wetted with liquid gold. The needle is produced from a rolled 1-mm-diam tungsten pin by slow ac etching in a 2M potassium hydroxide (KOH) solution. This process produces a 20° cone which terminates in a rounded point with a radius of approximately 10 μm. Though the tip radius [19] influences the emission characteristics of the LMIS, in practice it is easy to compensate for variations in the source performance (e.g., the emission threshold voltage) due to differing tip radii by varying other experimental parameters such as the distance between the needle tip and the extraction electrode.

In the source, the base of the needle is mounted to an electrically isolated copper support to which a bias voltage (typically, $V_{bias} = 150–300$ V) is applied. The body of the needle extends through a ceramic reservoir holdings about 5 mm^3 of gold and the assembly is heated by external tantalum wire heaters. Exterior insulators and heat shields are employed to reduce the heat load on the vacuum chamber walls. The principal advantages of the reservoir system [22] are that evaporation of the source metal is limited and that a relatively greater quantity of metal is put at disposition. The estimated lifetime of the present source, limited by the quantity of liquid metal, is 2000 h.

The source-heater assembly is mounted on a three-axis mount for precise positioning of the source with respect to the lens axis during source operation. The cluster ion beam is focused by a low chromatic aberration asymmetric triode lens system [33]. Two orthogonal sets of parallel-plate deflectors steer the beam precisely into the entrance of the energy filter and mass spectrometer (discussed below). Typically, in operation, the needle tip is located 0.5 mm from the face of the extractor electrode, and the source is operated at a total emission current of 10 μA to optimize the detected intensity of large doubly charged clusters.

B. Energy filter and mass spectrometer

The general layout of the experiment is shown in Fig. 2. After a free flight of 70 cm, the ions are focused by a second set of electrostatic lenses into the entrance of a 90° parallel-plate electrostatic energy filter [34]. A parallel-plate design was selected for ease of construction and high transmission. The principal function of the filter is to tighten up the otherwise broad distribution of ion kinetic energies coming from the source. The design resolution of the filter is 10%, and comparable resolution is obtained in practice. Turning the ion beam through a 90° angle has the additional advantage of efficiently suppressing energetic ions and fast neutral particles emitted by the source. Both of these contributed to a significant detector background when the source was mounted at the entrance of and coaxial with the mass spectrometers.

The triple quadrupole mass spectrometer, based on commercially available instruments, is described in detail elsewhere [3]. The first quadrupole Q1 is 20 cm in length and has a mass range of approximately 2000 amu. Q1 is used to select a particular n/z (mass-to-charge ratio) for experimentation. The second quadrupole Q2, which is operated as a nondiscriminating ion guide, has a length of 60 cm. While the clusters are in this guided drift region, they collide with gas atoms or absorb photons. The third quadrupole Q3, modified to extend its mass range to over 4000 amu, is used to analyze the charged cluster fragments emerging from Q2. The large mass range of Q3 is necessary to detect fragments from highly asymmetric fission reactions.

Some care must be exercised in recording dissociation spectra of multiply charged clusters. Instrumental distortions due to mass- and energy-dependent transmission

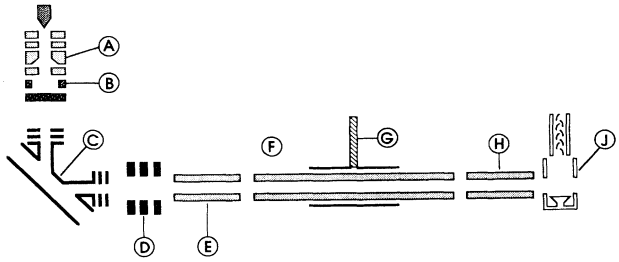

FIG. 2. The layout of the cluster source and the triple quadrupole mass spectrometer. The labeled components are A, the LMIS; B, beam deflectors; C, parallel-plate electrostatic energy filter with input and output trim lenses; E, Q1, F, Q2, G, gas inlet, and H, Q3; and J, the Daly conversion dynode and secondary electron multiplier. The lengths of Q1 and Q3 are 20 cm. Q2 has a length of 60 cm.

could systematically alter the appearance of the spectra. To guard against such systematic errors, (1) the mass spectrometers were always run at the lowest possible resolution and (2) the kinetic energy of the ions in the third quadrupole was scanned with the mass to ensure that the kinetic energies of the ions in the spectrometer remained constant (approximately 20 eV) for all detected masses. The variation of fragment kinetic energies is easily derived from momentum-conservation arguments and results in fragment kinetic energies which scale linearly with the fragment mass and inversely with charge.

Ions are converted to secondary electrons by a high-voltage Daly dynode. The dynode voltage (typically, $V_{\text{dynode}} = -20$ kV) is adjusted to optimize between a high ion counting rate on the one hand and a low detector background (typically, 1–5 counts/s) on the other. At this voltage the relative intensities of the cluster ions do not depend strongly on the dynode voltage, indicating that the detection efficiency is largely independent of the cluster mass. Electrons from the dynode are amplified by a standard secondary electron multiplier. The resulting pulses are amplified, shaped, and discriminated before being counted and stored by a laboratory computer.

A cluster mass spectrum over the range of interest in the present study is shown in Fig. 3. Doubly charged clusters, above Au_9^{2+}, increase in intensity rapidly with increasing size. While one might infer on the basis of this mass spectrum that the critical size is Au_9^{2+}, this would in fact be incorrect. Under slightly different experimental conditions, very weak signals at Au_7^{2+} and Au_5^{2+} are detectable [25]. Thus, *all* sizes of doubly charged Au clusters are present in the mass spectrum, from the dimer up. Triply charged clusters are visible above about Au_{26}^{3+}.

The kinetic-energy distribution of the ions has some relevance to the mechanism of cluster production by the LMIS. Kinetic-energy spectra, measured for ions Au^{2+}, Au_7^+, and Au_{15}^{2+}, are shown in Fig. 4. In these measurements, $V_{\text{bias}} = 175$ V. The spectra are recorded by scanning the pass energy of the energy filter while keeping other experimental parameters constant. From the figure it is evident that cluster ions Au_7^+ and Au_{15}^{2+}, have a broad energy distribution whose width is substantially in excess of that of Au^{2+}. As Au^{2+} is not a probable fragmentation product (on energetic grounds), its energy distribution closely mirrors that due simply to the source bias voltage and space-charge effects in the vicinity of the emission region. On the other hand, the excess energy (rather than deficient energy) of the cluster ions relative to Au^{2+} suggests that they are products of fission reactions (from highly charged parent clusters) rather than evaporation products of species with the same charge. This suggests that the primordial clusters produced by the LMIS are highly charged and lose their excess internal energy predominantly through fission rather than evaporation. This conclusion is in substantial agreement with van de Walle and Joyes (Ref. [29]), but at odds with conclusions drawn elsewhere [36].

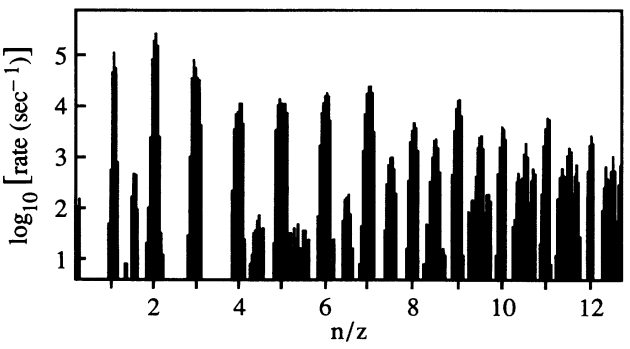

FIG. 3. A mass spectrum of the multiply charged clusters produced by the LMIS when the ion-pass energy is set about 30 eV above the needle bias energy. The intensity of the doubly charged clusters decreases quasiexponentially below about $n/z = 8$.

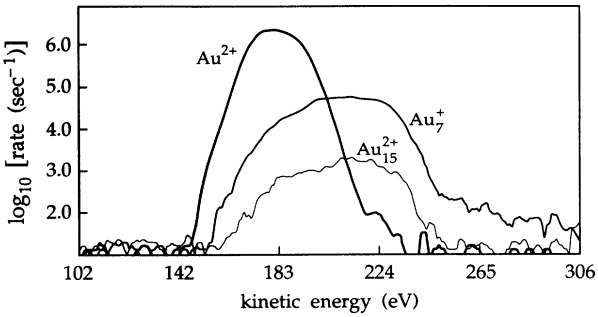

FIG. 4. Measured energy distribution for the Au_n^{z+}. Note the log scale. The doubly charged atom (Au^{2+}) has a sharp distribution centered at the needle bias voltage with a width which is essentially that of the energy filter. The energy distribution of the clusters is shifted *higher* energy, indicating that they are products of fission reactions, and not products of evaporation reactions, which on the basis of elementary considerations, would result in a lower kinetic energy.

III. EXPERIMENTAL RESULTS

The present experiments rely on the behavior of the multiply charged clusters when they undergo fragmentation to convey information about their physical properties. Here, fragmentation of the metal clusters is induced by both collisions with inert gas atoms and by photoabsorption. The fragmentation spectra are recorded by (1) selecting a parent cluster (n/z) with Q1, (2) allowing it to undergo interactions or fragmentation in Q2, and (3) analyzing the fragments with Q3. Products of both fission and evaporation reactions are observed with varying relative probabilities (depending on the parent cluster size). Of primary interest in these studies are the branching ratios between the fission and evaporative decay channels. As shall be discussed in Sec. V, the branching ratio, and its behavior with cluster size, can be correlated to prediction of the liquid-drop model.

Some ambiguity is unavoidable in measurements on multiply charged clusters because mass spectrometers distinguish ions only by their mass-to-charge ratio, n/z. If an ion has a half-integral n/z, it is certainly doubly

charged (admitting it is not quadruply charged) and so doubly charged clusters with half-integral n/z can be cleanly separated from other species for experimentation. The ambiguity arises for ions with integral n/z. In the mass spectrum of Fig. 3, the intensity of the singly charged clusters is greater than that of the (half-integral n/z) doubly charged clusters for $n/z < 10$ and, in likelihood, also that of the integral n/z doubly charged clusters. Thus, doubly charged clusters with integral n/z cannot be cleanly separated from the overlapping singly charged cluster. Despite this, however, useful measurements can be performed on these latter clusters by recognizing that both the doubly charged evaporation product (which will have a half-integral n/z) and the heavier asymmetric fission products (which will have an n/z *greater* than that of the parent) can be uniquely attributed to the (unobserved) doubly charged parent. Singly charged products of symmetric fission cannot be observed. However, as discussed below, there is considerable circumstantial evidence that symmetric fission is not a probable reaction for the size ranges and collision energies considered here.

A. Collision-induced fission

Collisional excitation of the clusters is carried out in Q2 by passing the ion beam through a region into which a target gas, typically Kr, has been introduced. The laboratory kinetic energies of the ions while in Q2 can be varied continuously between 0 and 600 eV. The Kr pressure P_{Kr} is typically between 10^{-6} and 2×10^{-5} mbar.

Typically dissociation spectra for the Au_n^{2+}, with $9 \le n \le 17$ (except for Au_{11}^{2+} and Au_{13}^{2+}) are shown in Fig. 5. The spectra were recorded at a laboratory energy of approximately 300 eV and with $P_{Kr} \approx 10^{-5}$ mbar. As discussed above, the half-integral n/z clusters can be cleanly separated by Q1 for subsequent experimentation. Thus, all products shown in the spectra of these clusters are due solely to the parent cluster in question. For Au_{17}^{2+}, the dominant reaction product is from the evaporation of a neutral atom, i.e., Au_{16}^{2+}. Au_{15}^{2+} and Au_{14}^{2+}, in rough proportion of equal intensity, are also observed. Pressure-dependence measurements (discussed below) show that these reaction products are due primarily to one-collision excitation of the parent cluster.

Apart from the evaporation products, weak signals at Au_3^+ and Au_{13}^+, due to the fission decay of Au_{17}^{2+}, are visible. The total mass of the parent cluster is not accounted for in the charged products and so the most reasonable assumption is that the fission reaction of Au_{17}^{2+} is accompanied by evaporation of a neutral atom:

$$Au_{17}^{2+} \rightarrow Au_{13}^{2+} + Au_3^+ Au \ . \quad (1)$$

It is not possible, with the present experimental configuration, to tell whether the neutral atom is emitted by Au_{17}^{2+} prior to fission or evaporated by a charged fragment subsequent to fission; however, measurements of the collision-energy dependence of the fragmentation branching ratios, discussed below, suggest that evaporation precedes fission.

Au_{16}^{2+} cannot be cleanly separated from Au_8^+ by the mass spectrometers, because of the equality of their n/z. Nevertheless, when $n/z = 8$ is selected by Q1, some of the fragments observed by Q3 are ascribable only to the parent cluster Au_{16}^{2+}. For instance, fragment signals at Au_{15}^{2+}, Au_9^+, and Au_{11}^+ cannot come from the fragmentation of Au_8^+. In the spectrum shown, there is apparently a very weak peak at Au_{15}^+; however, the signal is not reproducible and must, in the present case, be attributed to detection noise. Efforts to enhance or duplicate this signal were not successful. Thus, Au_{16}^{2+} undergoes the fission reactions

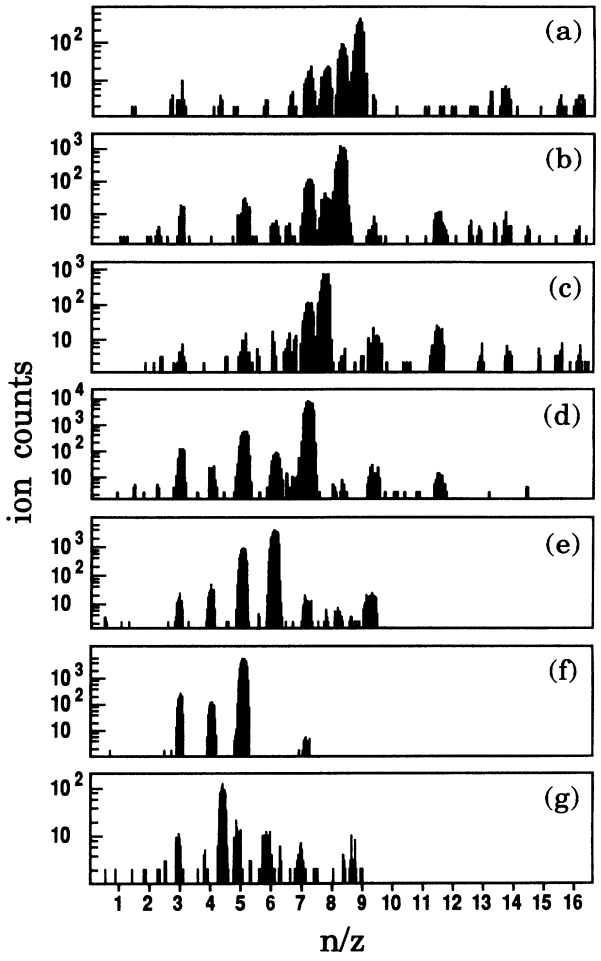

FIG. 5. Fragmentation spectra of the multiply charged Au clusters. (a) Parent cluster Au_{17}^{2+}. The predominant fragmentation pathway is evaporation. Some products from multiple evaporative steps are apparent. (b) Parent clusters Au_{16}^{2+} and Au_8^+. The evaporation product at $n/z = 7.5$, corresponding to Au_{15}^{2+} and the fission products with $n/z > 8$, are due to Au_{16}^{2+}. (c) Parent cluster Au_{15}^{2+}. Evaporation and fission products are apparent. (d) Parent clusters Au_{14}^{2+} and Au_7^+. The evaporation product Au_{13}^{2+} and the fission products with $n/z > 7$ are due to Au_{14}^+. (e) Parent clusters Au_{12}^{2+} and Au_6^+. Only fission products from the multiply charged cluster can be assigned unambiguously to it. (f) The parent clusters Au_{10}^{2+} and Au_5^+. Only a weak fission fragment at Au_7^+ is apparent. (g) Parent cluster Au_9^{2+}. Only fission products have measurable intensities. No evaporation channel is observed.

$$Au_{16}^{2+} \rightarrow Au_{13}^{+} + Au_3^{+} , \quad (2)$$

$$Au_{16}^{2+} \rightarrow Au_{11}^{2+} + Au_5^{+} , \quad (3)$$

as well as the evaporation reaction

$$Au_{16}^{2+} \rightarrow Au_1^{2+} + Au . \quad (4)$$

Au_{15}^{2+} and Au_{14}^{2+} show behavior similar to that of Au_{17}^{2+} and Au_{16}^{2+}, respectively. The smallest observed fission fragment is Au_3^{+} in both cases. The strengths of the fission signals relative to the evaporation signals are increased considerably. Also, the relative intensities of the more symmetric reactions increase relative to the less symmetric ones.

For the smaller clusters, Au_{12}^{2+}, Au_{10}^{2+}, and Au_9^{2+}, evaporation signals are not strong enough to be observed in these spectra. By accumulating signal at a fixed channel position, a very weak evaporation signal from Au_{12}^{2+} is detectable, but for the rest the combined effects of weak parent intensity and low evaporation probability make evaporation signals undetectable. For Au_9^{2+}, a weak but reproducible signal from the fission fragment Au_7^{+} is observed. This is the only fission reaction for which (indirect) evidence of a fission product smaller than Au_3^{+} is observed. The corresponding light fragment, i.e., Au^{+} or Au_2^{+} was not detected, probably because its kinetic energy exceeded the effective confinement potential of the ion guide.

The kinetic-energy dependence of the relative fragmentation branching ratios for several reactions are shown in Figs. 6–9 along with the measured distributions of parent-cluster kinetic energies in two of the cases. The data were recorded by scanning the bias potential of Q2 while monitoring the individual fragment intensities at 300 individual points between the limits of the scan. The distribution of the parent-ion kinetic energies, the derivative of the parent-cluster transmission as a function of the Q2 bias voltage, ultimately limits the resolution of the measurement. The center-of-momentum collision energy $E_{c.m.}$,

$$E_{c.m.} = zV_{rel}[M_{Kr}/(nM_{Au} + M_{Kr})] , \quad (5)$$

where V_{rel} is the bias voltage relative to the center of the parent-ion kinetic-energy distribution and $M_{Au} = 197$ and $M_{Kr} = 83.8$ are the masses of an Au atom and a Kr atom, respectively, in amu, is also shown. The zero of the c.m. collision energy is chosen to be the peak of the parent-cluster kinetic-energy distribution.

Because of the high internal excitation of the clusters, the thresholds for collision-induced fragmentation show a characteristic "zero-threshold" behavior, already discussed in connection with fission measurements on smaller multiply charged Au clusters [37]. It is not possible, at

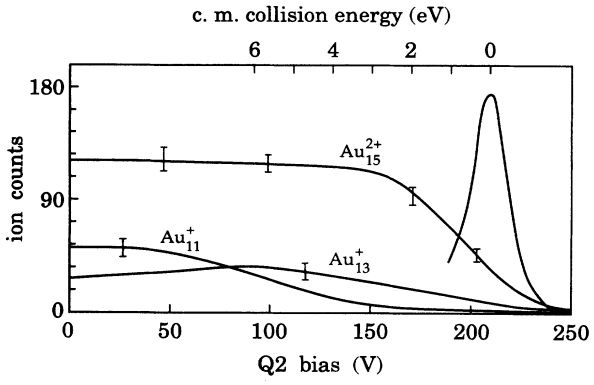

FIG. 6. The collision-energy dependence for the dominant fragmentation products of Au_{16}^{2+}. The Q2 bias voltage is shown on the bottom scale, and the computed center-of-momentum collision energy is shown on the top. The zero is chosen to coincide with the peak of the parent-ion kinetic-energy distribution. The signals for the fission products were integrated ten times longer than that of the evaporation product. See the text for discussion of the error bars. The width of the measured distribution of the parent-cluster ion kinetic energies corresponds to the resolution of the ion-energy filter.

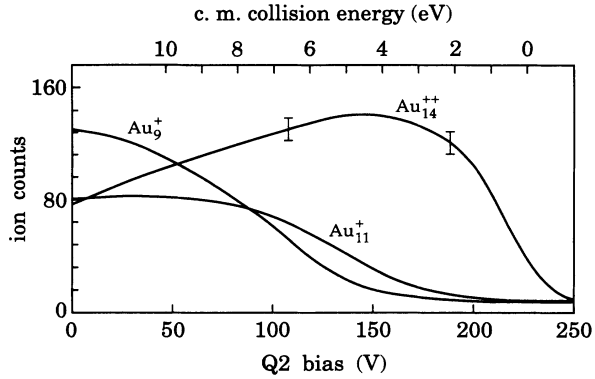

FIG. 7. The kinetic-energy dependence of the fragmentation channels of Au_{15}^{2+}. In this case, typical of the n-odd clusters, the evaporation product intensity clearly shows a lower collision-energy threshold than do the fission reactions. At higher energy, the evaporation product intensity drops as the fission channels open. The fission product intensities were integrated ten times longer than the evaporation product intensity.

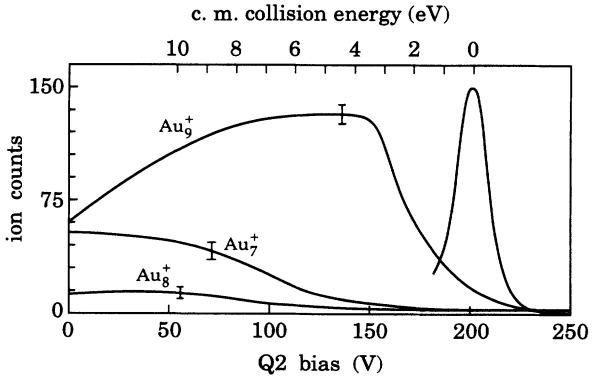

FIG. 8. The kinetic-energy dependence of the fragmentation channels of Au_{12}^{2+}. For Au_{12}^{2+} the dominant fragmentation channels are via fission. The lowest threshold channel is to $Au_9^{+} + Au_3^{+}$. The other fission products have threshold energies which are 4–6 eV above that threshold.

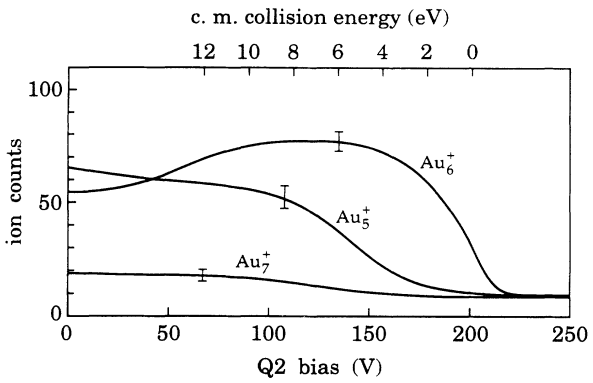

FIG. 9. The kinetic-energy dependence of the fission reactions of Au_9^{2+}. The channel to $Au_6^+ + Au_3^+$ has the lowest threshold energy. The other reactions have thresholds that are 4–6 eV higher. The channel to Au_7^+ is the only channel observed in these measurements which can be identified with fission to a charged product with fewer than three atoms.

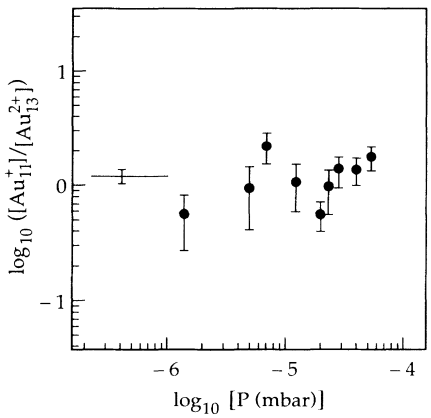

FIG. 10. The ratio of the dominant evaporation and fission product intensities for Au_{14}^{2+} as a function of the gas pressure P. The ratio is largely independent of the gas pressure. The average value and its error is shown to the left.

the present level of precision, to measure directly the differences between the thresholds for evaporation and fission in the most interesting cases (those of the n-even clusters). Nevertheless, these measured spectra do contain information which is instructive in the analysis of the data.

The kinetic-energy dependence of the relative fragment intensities for Au_{16}^{2+} are shown in Fig. 6. The signals for the fragments Au_{11}^+ and Au_{13}^+ were accumulated 10 times longer than the signal for Au_{15}^{2+}. Rather than plot the individual data points, which contain considerable scatter, a smoothed line has been drawn through the points, and, at several points, error bars which represent the standard deviation about the average of ten channels are shown. The distribution of parent-ion kientic energies is shown for comparison.

The data show that the thresholds for both evaporation to Au_{15}^{2+} and fission to Au_{13}^+ are indistinguishable at the present level of precision. Nevertheless, the measured curves are slightly different. The evaporation channel rises steeply to a saturated value near a c.m. collision energy of 3 eV. The Au_{13}^+ intensity rises more slowly and reaches its maximum value around 6 eV. On the other hand, the threshold for the channel to Au_{11}^+ is substantially higher (2–4 eV) than those for the other channels. As the Au_{11}^+ intensity rises, the intensity of the Au_{13}^+ channel decreases slightly, whereas the evaporation product intensity remains constant.

For Au_{15}^{2+} (Fig. 7) the evaporation channel (Au_{14}^{2+}) clearly has the lowest threshold energy. Only for collision energies above the 4-eV range do the fission product intensities begin to contribute significantly to the fragmentation spectrum. This behavior is typical of the n-odd doubly charged clusters with $n > 13$. Namely, the evaporation channels have a much lower threshold energy than do the fission channels.

In Figs. 8 and 9 the kinetic-energy dependences for Au_{12}^{2+} and Au_9^{2+} are shown. In both cases, the fission product which appears at the lowest collision energies is that which accompanies Au_3^+. Only for collision energies of 4–6 eV do other fission products appear with measurable intensities. The data for Au_9^{2+} are of interest because they show that the channel giving Au_7^+ has a significantly higher activation energy than the channel giving Au_6^+. The Au_7^+ channel is the only channel observed in these measurements which can be unambiguously identified with a fission reaction resulting in a charged product smaller than Au_3^+.

An important quantity to measure is the branching ratio between fission and evaporation. As is discussed below, this ratio gives direct information about the relative height of the fission barrier, which is expected to depend strongly on cluster size. To verify that multiple collisions do not introduce spurious effects in the measurements of the ratio, the pressure dependences of most of the important fragmentation reactions were measured. In Fig. 10 the pressure dependence of the ratio of the evaporation product intensity to the main fission product intensity for the parent cluster Au_{14}^{2+} is plotted as a function of P_{Kr}. While the scatter of the data is somewhat higher at low pressure (because of a lower interaction probability and hence a lower fragment signal), the ratio is independent of pressure, within experimental error. Similar data for the parent cluster Au_{18}^{2+} are plotted in Fig. 11. Again, the scatter in the data is large for $P_{Kr} < 3\times10^{-5}$ mbar, but the results are independent of pressure. For $P_{Kr} > 5.5\times10^{-5}$ mbar, however, the ratio of the evaporation and fission product intensities shows some pressure dependence, primarily due to subsequent fission of the evaporation product due to multiple collisions with the background gas. In both Figs. 10 and 11 the average of the data for pressures below 3×10^{-5} mbar is shown.

Summing the fission product intensities for a particular cluster and dividing by the evaporation product intensity gives the branching ratio (relative fission rate) Γ_f/Γ_e. The measured values of Γ_f/Γ_e for the Au_n^{z+} are plotted as a function of z^2/n in Fig. 12 for two laboratory collision energies. As discussed in Sec. II, some care must be taken to suppress systematic effects such as mass-dependent transmission and detection which could lead

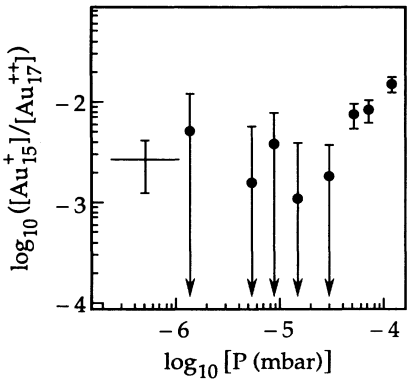

FIG. 11. The measured ratio of the dominant fission and evaporation product intensities for Au_{18}^{2+}. The ratio is independent of pressure at low pressures, where multiple collision effects are unimportant, while at higher pressures, the signal becomes pressure dependent. Low signal levels contribute to large uncertainties at low pressures. The average of the points below $P=3\times10^{-5}$ and its error is shown.

to distortions of the measured decay rates. The measured values reported here are the averages of several (between three and eight) experimental runs. Typically, Γ_f/Γ_e varied no more than a factor of 3 for any individual cluster between given runs. The error bars reflect only the random error in the measurements—systematic effects, such as the inability to observe unambiguously the charge of n-even products, are not considered. The similarity of Fig. 12 to a similar graph [38] of nuclear fission rates is discussed in Sec. V.

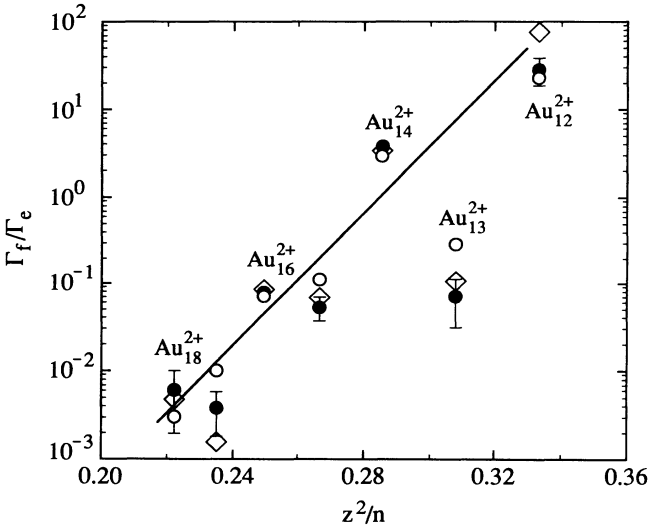

FIG. 12. The relative fission rate Γ_f/Γ_e for the multiply charged Au clusters n^{z+} as a function of z^2/n. Data points for collision-induced dissociation at laboratory energies of 400 eV (○), 200 eV (●), and fission induced by a 2.41-eV photon (◇) are shown. The quasiexponential dependence on z^2/n is a strong indicator of liquid-drop-like behavior in the clusters.

B. Photoinduced fission

The branching ratios for photoinduced fission and evaporation were determined in a manner similar to that employed above, the most substantial difference being that instead of running the ions through Q2 at high kinetic energies, the lowest possible kinetic energies in Q2 are used which ensures a high ion transmission while maximizing the interaction time of the clusters with the coaxial beam of an Ar-ion laser. Typically, the laboratory kinetic energies of the ions were between and 10 eV.

A single excitation wavelength, the 14-nm line of the Ar-ion laser, was used. This wavelength overlaps the (broad) plasmon absorption of large supported Au clusters [39]. Detailed gas-phase measurements for the plasmon absorption of small Au cluster ions are not available; thus, it is not certain to what extent our excitation wavelength overlaps the plasmon peak. However, the total fragmentation cross sections in all cases are roughly a factor of 100 below the peak plasmon absorption cross section of K_{20}^+ as measured on the same apparatus [40], suggesting that the plasmon energy in these small clusters may be substantially shifted from those of supported clusters.

From the data for the photoinduced fission, the relative fissionability Γ_f/Γ_e is determined in a similar manner as in the case of collision-induced fission. These data are included in Fig. 12 for comparison.

IV. THE LIQUID-DROP MODEL

Cluster fission is a collective phenomenon. Therefore, it is logical to consider it within a framework like the liquid-drop model, which emphasizes the motion of the cluster surface while ignoring the less important (and more complicated) motions of individual atoms within the cluster. The analogy between a cluster and a liquid drop is justified by the cluster's approximately constant density and its sharp boundary. The model does not address low-temperature behavior, such as crystalline structure. Rather, the model is useful in predicting the behavior of clusters excited above their fragmentation thresholds. A simple estimate shows that for an excitation energy of 3 eV, a cluster with 20 atoms will have a temperature corresponding to 600 K, well above its melting point [41].

The liquid-drop model, in the form most useful for describing fission, originates in the work of Rayleigh [42] on the surface modes of charged macroscopic liquid droplets. It was found that a given droplet is unstable to spontaneous (fission) decay if the charge on it is too great. The situation of a fixed charge and decreasing droplet mass, more pertinent in the present context, is functionally equivalent.

The implications of the liquid-drop model have been considerably refined and extended through its application to nuclear fission [43,44]. Bohr and Wheeler [43] developed the model to the point of predicting fission-barrier heights, and their work has served as the cornerstone for most of the subsequent work.

In this section the application of the liquid-drop model to conducting metallic droplets is discussed. An intro-

ductory review is given for the sake of defining terms. It is shown in the Appendix that the Coulomb contribution to the deformation energy of a conducting metallic droplet differs only slightly from that of a uniformly charged droplet. Thus, the implications of the liquid-drop model regarding fission-barrier heights of charged clusters are discussed largely on the basis of existing literature regarding nuclear fission.

The liquid-drop model is based on the assumption that the total cluster energy can be written as the sum of Coulomb and surface contributions:

$$E_T = E_b + E_s + E_C \ , \tag{6}$$

where E_b is the bulk (volume) energy, E_s is the surface energy, and E_C is the Coulomb energy. E_b is taken, within this approximation, to be the number of atoms in the cluster times the bulk cohesive energy of the metal. It is assumed to be independent of the droplet shape. E_s and E_C, on the other hand, are shape dependent. To calculate them, the standard parametrization [44] of the droplet surface, r_d,

$$r_d = a[1+\alpha_0 P_0(\cos\theta)+\alpha_2 P_2(\cos\theta)] \ , \tag{7}$$

is adopted, where $a = r_0 n^{1/3}$, with r_0 the atomic radius and n the number of atoms in the cluster. The α_l are the deformation parameters and the P_l are Legendre polynomials of order l. The term α_2 in (7) is the quadrupolar surface deformation parameter. This parameter is of greatest importance in the initial stages of fission. The parameter α_0 is included in the expansion to conserve the cluster volume. Taking

$$\alpha_0 = -\alpha_2^2/5 - 2\alpha_2^3/105 \tag{8}$$

conserves the cluster volume to fourth order in α_2.

E_s is evaluated under the assumption that the surface energy is proportional to the surface area of the deformed cluster. This gives [45]

$$E_s = \varepsilon_{s0} n^{2/3}(1+\tfrac{2}{5}\alpha_2^2 - \tfrac{4}{105}\alpha_2^3 - \tfrac{38}{175}\alpha_2^4) \tag{9}$$

to fourth order in α_2. Here, $\varepsilon_{s0} = 4\pi r_0^2 \sigma$, where σ is the surface tension of the droplet. For the present purposes, curvature corrections [46] to the droplet surface tension are ignored and the bulk value is taken.

It is shown in the Appendix that, to fourth order in α_2, E_{C0} for a conducting metallic droplet is given by

$$E_C = z^2 \varepsilon_{C0} n^{-1/3}(1 - \tfrac{1}{5}\alpha_2^2 - \tfrac{4}{105}\alpha_2^3 + \tfrac{53}{245}\alpha_2^4) \ , \tag{10}$$

where $\varepsilon_{C0} = e^2/(2r_0)$. This expression is the same as that for a uniformly charged (nonconducting) droplet to third order in α_2. The coefficient of the fourth-order term for a nonconducting droplet is $\frac{157}{1225}$. The smallness of the difference between the deformation energies of conducting and insulating droplets is a surprising result. This explains why a straight adaptation of the nuclear formulas to cluster-fission-barrier heights [47,48] gives reasonable agreement with experiment.

Combining Eqs. (9) and (10), it is evident that for

$$z^2 \varepsilon_{C0} n^{-1/3} = 2\varepsilon_{s0} n^{2/3} \ ,$$

the stabilizing force of the surface tension is just balanced by the destabilizing force of the Coulomb repulsion. This implies that when

$$\left[\frac{z^2}{n}\right] \equiv \left[\frac{z^2}{n}\right]_c = 2\varepsilon_{s0}/\varepsilon_{C0} = 12(4\pi r_0^3/3)\sigma/e^2 \ , \tag{11}$$

the droplet is unstable to spontaneous fission, even at zero temperature. The size given by $n_c^{z+} = z^2/(z^2/n)_c$ is defined for the present paper as the critical size. This usage is consistent with the original definition by Sattler *et al.* Notice that the critical size for metallic clusters scales like z^2, as for van der Waals clusters.

TABLE I. $(z^2/n)_c$ and other relevant parameters for several metallic elements.

Element	r_0 (Å)[a]	σ (dyn cm^{-1})[b]	$(z^2/n)_c$
Ag	1.60	907	0.82
Au	1.59	1130	0.97
K	2.57	110	0.44
Na	2.08	203	0.39
Pb	1.93	388	0.71
In	1.84	514	0.76

[a]C. Kittel, *Introduction of Solid State Physics*, 5th ed. (Wiley, New York, 1976), p. 154.
[b]*CRC Handbook of Chemistry* and *Physics* (CRC, Palm Beach, FL, 1978), p. F-25.

The $(z^2/n)_c$ for several metallic elements are tabulated, along with the relevant parameters, in Table I. Notice that despite pronounced variations of the surface energies and atomic radii, the values of $(z^2/n)_c$ vary remarkably little for the metallic elements. For droplets with $z=2$, this implies that the critical sizes n_c^{2+}, lie between 4 and 12. In this size range the liquid-drop model is of limited validity. Molecular structure, which depends on the detailed arrangements of the atoms, dominates in the size range below about six atoms. The liquid-drop model is certainly not a reliable indicator of molecular behavior. Indeed, the experimental observation of multiply charged metallic dimers, well below n_c^{2+}, bears this out.

Nevertheless, while the critical size $(z^2/n)_c$ does not have direct physical significance regarding the behavior of small clusters, it does have physical significance as a scaling parameter in describing the behavior of larger clusters within the framework of the liquid-drop model. Properties of interest for the present analysis depend on the dimensionless fissionability parameter

$$x = (z^2/n)/(z^2/n)_c \ . \tag{12}$$

Evidently, for clusters of interest, $0 \le x \le 1$. In terms of the fissionability parameter, the total deformation energy of the clusters is

$$E_d = \varepsilon_{s0} n^{2/3}[0.40(1-x)\alpha_2^2 - (0.0381+0.0762x)\alpha_2^3 - (0.217-0.433x)\alpha_2^4] \ . \tag{13}$$

A. Fission barriers

The derivative of E_d vanishes, by definition, at the fission saddle point. The value of E_d there is the fission-barrier height. Once the droplet exceeds the saddle-point deformation, it is irreversibly destined to fission. The fission-barrier height is easily calculated in the limiting cases $x \ll 1$ and $(1-x) \ll 1$, whereas in the case more pertinent to experiment, that of x between about 0.3 and 0.5, the barrier height is more difficult to derive. As an approximate approach, the barrier heights can be derived in the two limiting cases within the conducting liquid-drop model. Both expressions are found to be close to those corresponding to the case of a nonconducting droplet. In the intermediate case, an interpolated formula is found which joins smoothly with the formulas appropriate for large and small x.

In the limit $(1-x) \ll 1$, the fission barrier is obtained from Eq. (13) by finding its stationary point and evaluating the energy there. Keeping terms to third order in α_2, this gives the familiar Bohr-Wheeler formula

$$\xi = \tfrac{98}{135}(1-x)^3 , \tag{14}$$

where the fission barrier is $E_f = \varepsilon_{s0} n^{2/3} \xi$. This expression is accurate to about 10% (compared to more complete numerical results) within the range $0.7 < x < 1.0$ (Ref. [49]).

In the limit $x \ll 1$, the saddle point is, to first approximation, two touching spheres. The energy is given by the difference between the total energies of the two fragments and the parent cluster, plus the interaction energy of the two touching spheres. In taking a simple point-charge interaction between the touching fragments, the only significant change to the Bohr and Wheeler result is that the interaction energy, relative to the Coulomb self-energy, is increased slightly. One obtains for the fission-barrier height in that case,

$$\xi = 0.2599 - 0.1102x . \tag{15}$$

Assuming that the cluster fragments are metallic, however, implies a lower interaction energy due to screening. For point charges with polarizability α, separated by distance R, the interaction energy is

$$W = e^2/R - 2\alpha(e/R^2 - 2p/R^3)^2 + 2p^2/R^3 , \tag{16}$$

where

$$p = \alpha(e/R^2)(1+2\alpha/R^3)^{-1} . \tag{17}$$

Taking the polarizability to be that of a classical metallic sphere, the fission-barrier height in the limit $x \ll 1$ is therefore

$$\xi = 0.2599 - 0.1983x . \tag{18}$$

This expression is close to that of a nonconducting droplet. The intercept is the same, and the slopes differ by less than 10%.

In the limiting cases of x, the fission-barrier heights for conducting droplets are very close to those derived for nonconducting (uniformly charged) droplets. This suggests that for intermediate values of x, the barrier heights for conducting and nonconducting droplets should also be comparable. It is reasonable, therefore, to adopt the interpolation scheme employed by Swiatecki [45] for the fission-barrier height for $x < 0.6$. In the present case, the function

$$\xi = 0.2599 - 0.1983x - 0.5369x^2 + 0.4575x^3 \tag{19}$$

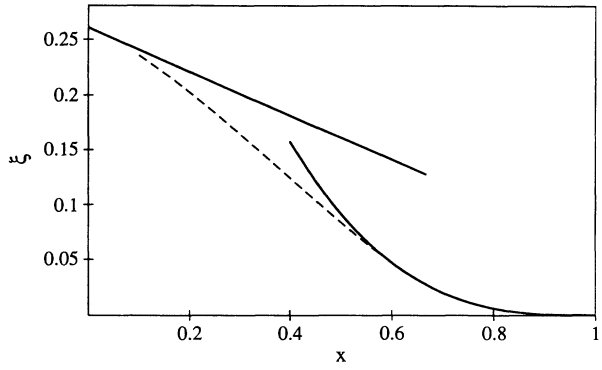

FIG. 13. The dimensionless fission barrier ξ as a function of the fissionability parameter x. The asymptotic curves, derived analytically in the limits $x \ll 1$ and $(1-x) \ll 1$ are shown. The interpolation formula, Eq. (19), is also shown (— — —).

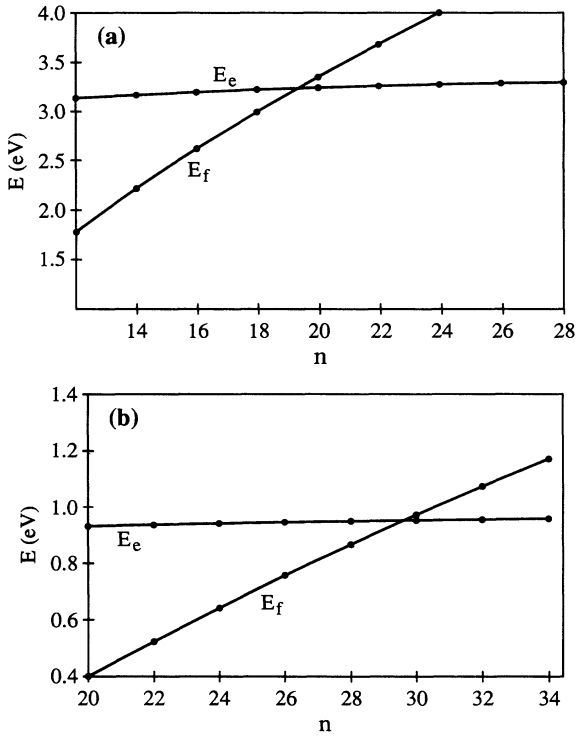

FIG. 14. (a) The fission-barrier height E_f and the evaporation energy E_e calculated from the liquid-drop model for Au clusters. The fission-barrier height crossed the evaporation energy above Au_{18}^{2+}. (b) The fission-barrier heights and evaporation energies for Na clusters. Here, the fission-barrier height crosses near Na_{30}^{2+}. The crossing point occurs at a larger size in Na than in Au due mainly to the lower surface tension of Na.

has the correct limiting behavior as x tends to zero and joins the expression (15) for the barrier height smoothly (equal value and first derivative) at $x=0.6$. This choice is somewhat arbitrary, though the general trend of the result is not strongly affected by the choice within the range $x=0.6-0.7$.

The expressions for the fission-barrier heights derived above are plotted together in Fig. 13. The functions valid at the extrema of x are joined smoothly by the interpolated function. Both limiting expressions overestimate the barrier with respect to the interpolation formula in the middle range of x.

The fission-barrier heights, calculated using the interpolation formula derived above, for doubly charged Au and Na clusters are displayed in the Figs. 14(a) and 14(b). For comparison, the evaporation energy E_e, derived from expression (6),

$$E_e=\varepsilon_b-\tfrac{2}{3}\varepsilon_s n^{-1/2}+O(n^{-4/3}) , \tag{20}$$

with $E_b=\varepsilon_b n$, where ε_b is the bulk cohesive energy and $\varepsilon_s=\varepsilon_{s0}n^{2/3}$, is also shown.

For Au clusters, the calculated fission barrier is lower than the evaporation energy for sizes Au_{18}^{2+} and below. For the Na clusters, on the other hand, the fission barrier crosses the evaporation energies near Na_{30}^{2+}. The shift of the crossing point to larger sizes in the case of alkali metals is primarily a consequence of their lower surface tension [50]. These theoretical results are compared with the available experimental results in Sec. V.

V. INTERPRETATION AND DISCUSSION

The measurements presented in Sec. III show that within a narrow range of cluster sizes, between Au_{12}^{2+} and Au_{18}^{2+}, both fission and evaporation compete as decay channels for energetically excited clusters, with the tendency to fission increasing strongly as the cluster size decreases. The first datum to interpret is the appearance of the cluster mass spectrum, Fig. 3. Its appearance can be explained assuming that the clusters produced by the LMIS undergo at least one spontaneous decay in their flight between the source and the mass spectrometer.

The relatively sharp exponential decrease in the intensities of the doubly charged clusters below Au_{16}^{2+} is easily reconciled with the data in Fig. 12. As the tendency toward fission increases, the number of surviving doubly charged fragmentation daughters decreases. Considering the smallness of the branching ratio for evaporation below about Au_{12}^{2+}, it seems likely that doubly charged clusters below this size either result from the fission of triply or quadruply charged clusters or are produced directly by the source.

It is important to notice that the decrease in the intensities of the doubly charged clusters occurs well above the critical size. What is important for the interpretation of mass spectra is the variation of the branching ratio, which depends on the relative magnitude of the evaporation energy and the fission-barrier height. This underscores the importance of considering both quantities in interpreting mass spectra of strongly bound materials such as metallic clusters.

Considering the measured relative fission rates of Fig. 12, a strong odd-even oscillation is observed in the data. In the case of the n-odd clusters, Γ_f/Γ_e is considerably lower than for the neighboring n-even clusters. This is most probably due to an odd-even alternation in the binding energies [51] although the systematic effects in the measurement of Γ_f/Γ_e discussed above may be responsible to some extent. The energy dependence observed for the n-odd cluster fragmentation (Fig. 7) is consistent with this interpretation.

For the n-even clusters (Figs. 6 and 10) the thresholds for the fission and evaporation channels are indistinguishable from one another in the size range studied. Indeed, the difference between the evaporation energy and fission barrier predicted by the liquid-drop model is below the experimental resolution. Thus, quantitative comparison with the model cannot be made using the present experimental data, and we must resort to more indirect means.

In a first approximation the relative rates for fission and evaporation should depend exponentially on the energy difference between the activation energies for the two processes. Thus,

$$\Gamma_f/\Gamma_e=(g_f/g_e)\exp[-(E_f-E_e)/kT] , \tag{21}$$

where g_f and g_e are factors taking into account the degeneracies and frequencies associated with the decay modes, k is the Boltzmann constant, and T is an effective temperature. Taking the liquid-drop-model expression for E_c [Eq. (14)] and for the fission barrier, $E_f=\varepsilon_s n^{2/3}\xi$, with ξ taken from Eq. (20), the experimental Γ_f/Γ_e can be compared directly to (21) as shown in Fig. 15. For clarity, the averages of the data on collision-induced fission for the n-even doubly charged clusters are shown.

Assuming that g_f/g_e does not vary strongly with cluster size and is of order unity, the liquid-drop model apparently predicts either a fission barrier which is too low or else an evaporation energy which is too high for the Au clusters. We would expect the fission-barrier height

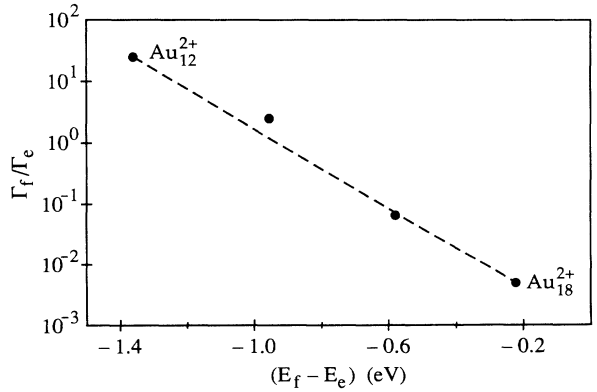

FIG. 15. The measured Γ_f/Γ_e for the multiply charged Au_n^{z+} as a function of the difference between the fission-barrier height and the evaporation energies predicted by the liquid-drop model. The straight line drawn between the data points has a slope, determined from the energy scale of the abscissa, corresponding to $kT\approx 1200$ K.

to equal the evaporation energy when Γ_f/Γ_e is of order 1. However, given that no adjustable parameters have been used in calculating the barrier heights or evaporation energies, the agreement with experiment must be considered as reasonable. Curvature corrections to the surface tension and electronic effects, both of which have been neglected in the present approximation, would tend to raise the surface energy and therefore bring the model into better agreement with experiment. From the slope of the line connecting the points in Fig. 15, one deduces on the basis of Eq. (23), $kT \approx 1200$ K. This value is reasonable, since it gives mean decay times which are on the same order as the flight times of the ions in the apparatus.

The liquid-drop model is generally applicable to metallic systems and should be useful for predicting the behavior of most families of metallic clusters. Unfortunately, detailed data on the branching ratios for other multiply charged metallic clusters are not available. However, the prediction of the model for Na clusters, shown in Fig. 14(b), is in good agreement with the limited data that are available [52]. In those experiments, the crossover from fission-dominated to evaporation-dominated decay is reported to be near Na_{30}^{2+}. This is in exact agreement with the predictions of the model. While such accuracy must be partly fortuitous, the correct prediction of the trend of the crossover point toward larger sizes in systems with lower surface tension strongly supports the thesis that the liquid-drop model is applicable to describing the fission of metallic clusters in general.

VI. CONCLUSIONS

The liquid-drop model provides a framework within which metallic-cluster fission can be understood on both a qualitative and a quantitative level. In particular, the observed increase in the cluster fissionability with decreasing cluster size is explained by the rapid decrease of the fission-barrier height with respect to the relatively constant evaporation energy. The model appears to be generally consistent with all available experimental data.

Two cluster sizes are important for characterizing the doubly charged clusters. The first, the critical size, is the cluster size for which the fission-barrier height (in the liquid-drop model) vanishes. While the critical size has significance in interpreting the mass spectra of multiply charged van der Waals clusters, it has little direct relevance to metal-cluster mass spectra. Indeed, for metals the critical size usually falls in a range where the model's validity may be questioned (for doubly charged Au clusters, $n_c^{2+}=4$) due to the dominance of molecular properties. The greatest role of the critical size is indirect, as a scaling parameter for other quantities, such as the fission barrier derived from the liquid-drop model.

The second cluster size of importance is the crossing point of the fission barrier and the evaporation energy. In van der Waals systems, the evaporation energy is low enough that it can be considered as insignificant compared to the Coulomb energies involved. However, in metallic clusters, the relatively greater strength of the atomic bonding leads to a crossing point which is far away from the critical size. Unlike the critical size, the crossing point can be measured directly by experiment, and thus provides a quantitative test for the model.

As successful as the liquid-drop model is in describing and interpreting the experimental results presented here, it can be criticized on several points. Most notable is its poor convergence when expressed as a power series in the α_n [49]. Various alternative parametrizations of the droplet surface have been employed, with some improvement, though the basic conclusions derived from the model in the present form remain unchanged.

Tacit in the application of the liquid-drop model to the present problem is the assumption that the fission saddle point is represented, in a first approximation, by a symmetric deformation. Despite the fact that the final state of the clusters is highly mass asymmetric, this is probably a reasonable assumption given the success of the model. In the case of nuclei, a similar situation arises. However, the fissionability parameters x of clusters are considerably lower than those of nuclei. Whether instabilities toward deformations of higher order [49] occur at the saddlepoint or not is a point worthy of investigation.

Recently, electronic effects in fission [24] and fissionlike [53] reactions of metal clusters have also been studied using the jellium model and the local-density approximation. These calculations, while as yet applied only to highly asymmetric reactions (monomer ion and neutral monomer and dimer ejection), contain many of the salient features of the liquid-drop model and may be looked to for more refined results. Landman *et al.* (Ref. [25]) have extended the capabilities of *ab initio* molecular-dynamics simulations to the spontaneous fission of small multiply charged Na clusters with considerable success.

Indeed, considering that the model has no free parameters, is based on the bulk value of the surface tension, and has no molecular parameters as input, its predictive power for such small objects is remarkable. Conversely, one may conclude that the development of bulklike properties in metallic clusters is quite rapid and that, at sizes of 10 to 20 atoms, the bulk surface tension is largely obtained.

ACKNOWLEDGMENTS

The author gratefully acknowledges the help of Nico Dam in the later stages of the measurements presented here. This work was partially supported by the Swiss National Science Fund, Grant No. 20-26535.89.

APPENDIX: CONDUCTING LIQUID-DROP MODEL

1. Introduction

As a conceptual framework, the application of the liquid-drop model to metal-cluster fission is preceded by its application to the fission of nuclei and van der Waals clusters. While the application of the model to these systems shows great overall similarity, in detail there are some differences which warrant scrutiny. In particular, it is not evident *a priori* that the Coulomb contribution to the deformation energy of a metallic droplet should be the same as that of a uniformly charged droplet (i.e., nu-

clei) or that of one which has charges localized at its extremes (i.e., van der Waals clusters).

In a metallic cluster the excess charge is mobile, delocalized, and, due to metallic screening, resides on the cluster surface. When the cluster deforms, the charge will concentrate at points of high surface curvature, varying in a way that a uniform potential is maintained over the surface. Below, it is shown that the electrostatic contribution to the deformation energy of a metallic droplet has, apart from a constant factor, the same dependence on the quadrupolar surface deformation parameter that is found in the case of a uniformly charged droplet.

2. Conducting droplet electrostatics

Calculating the electrostatic contribution to the deformation energy amounts to solving Poisson's equation with Dirichlet boundary conditions for the deformed droplet. The solution of Poisson's equation in spherical coordinates which converges for $r \to \infty$ is

$$\Phi(r,\theta)=\sum_{l=0}^{\infty} B_l r^{-(l+1)} P_l(\cos\theta) , \tag{A1}$$

where $\Phi(r,\theta)$ is the electrostatic potential. The B_l are constants to be chosen such that the boundary condition at $r=r_d$, [Eq. (7)],

$$\Phi(r,\theta)=\Phi_0=\sum_{l=0}^{\infty} B_l a^{-(l+1)}[1+\alpha_0+\alpha_2 P_2(\cos\theta)]^{-(l+1)} \times P_l(\cos\theta) , \tag{A2}$$

where $\Phi_0=$ const, is satisfied.

Solving the infinite system of linear equations (A2) exactly is a tough problem. In practice, it is easier to solve the problem approximately by making two simplifying assumptions: (1) that we can cut off the series [Eq. (2)] at some suitably large value of $l=l_{\max}$ and (2) that we can expand the solution about $\alpha_2=0$. Taking $l_{\max}=8$ and keeping terms only up to fourth order in α_2, the first five nonzero coefficients are

$$B_0=a\Phi_0(1+\alpha_2^2/5+4\alpha_2^3/105-216\alpha_2^4/1225) , \tag{A3}$$

$$B_2=a^3\Phi_0(\alpha+4\alpha_2^2/7+9\alpha_2^3/49-22\,424\alpha_2^4/56\,595) , \tag{A4}$$

$$B_4=a^5\Phi_0(36\alpha_2^2/35+2196\alpha_2^3/2695 -421\,812\alpha_2^4/13\,488\,475) , \tag{A5}$$

$$B_6=a^7\Phi_0(90\alpha_2^3/77+35\,856\alpha_2^4/29\,645) , \tag{A6}$$

$$B_8=a^9\Phi_0(1008\alpha_2^4/715) . \tag{A7}$$

This solution gives a potential which is constant over the surface $r=r_d$ to order α_2^4.

The constant Φ_0, while independent of θ, must depend on α_2 to maintain a constant charge ze on the cluster surface. Taking the limit of (A2) as $r\to\infty$, we must have $\Phi(r,\theta)\to ze/r$. Thus, again to fourth order in α_2,

$$\Phi_0=\frac{ze}{a}(1-\alpha_2^2/5-4\alpha_2^3/105+53\alpha_2^4/245) . \tag{A8}$$

This result can also be derived using Gauss's law by integrating the normal component of the electric field over the surface of a volume much larger than the cluster. A straightforward calculation gives the total electrostatic energy of the sphere to be

$$E=\frac{z^2e^2}{2a}(1-\alpha_2^2/5-4\alpha_2^3/105+53\alpha_2^4/245) . \tag{A9}$$

Thus, the deformation energy for a conducting sphere is the same as that for the uniformly charged sphere, apart from the leading coefficient in the expansion, to lowest order in α_2.

The charge density on the cluster surface changes to compensate for the variation of the curvature over the surface. Taking the normal component of the electric field at the cluster surface, the surface charge density is, to lowest order in α_2,

$$\sigma=\frac{ze}{4\pi a^2}[1+2\alpha_2 P_2(\cos\theta)] . \tag{A10}$$

---

*Present address: Department of Applied Physics, Mail Stop 128-95, California Institute of Technology, Pasadena, CA 91125.

[1] O. Chesnovsky, K. J. Taylor, J. Conceicao, and R. E. Smalley, Phys. Rev. Lett. **64**, 1785 (1990).
[2] W. Ekardt, Phys. Rev. B **29**, 1558 (1984).
[3] D. Beck, Phys. Rev. B **30**, 6935 (1984); W. Ekardt, *ibid.* **31**, 6360 (1985).
[4] W. D. Knight, K. Clemenger, W. A. de Heer, and W. A. Saunders, Phys. Rev. B **31**, 2539 (1985).
[5] K. Sattler, J. Mühlbach, O. Echt, P. Pfau, and E. Recknagel, Phys. Rev. Lett. **47**, 160 (1981).
[6] O. Echt, in *Electronic and Atomic Collisions,* edited by H. B. Gilbody, W. R. Newell, F. H. Read, and A. C. H. Smith (Elsevier, New York, 1988), p. 719.
[7] O. Echt, in *Physics and Chemistry of Small Clusters,* edited by P. Jena, B. K. Rao, and S. N. Khanna (Plenum, New York, 1987), p. 623.
[8] O. Echt, D. Kreisle, E. Recknagel, J. J. Saenz, R. Caero, and J. M. Soler, Phys. Rev. A **38**, 3236 (1988).
[9] D. Kreisle, O. Echt, M. Knapp, E. Recknagel, K. Leiter, T. D. Märk, J. J. Saenz, and J. M. Soler, Phys. Rev. Lett. **556**, 1551 (1986).
[10] D. Tomanek, S. Muhkerjee, and K. H. Bennemann, Phys. Rev. **B28**, 665 (1983).
[11] R. Caero, J. J. Saenz, and J. M. Soler, Phys. Rev. A **37**, 1401 (1988).
[12] P. Pfau, K. Sattler, R. Pflaum, and E. Recknagel, Phys. Lett. A **104**, 262 (1984).
[13] W. Schulze, B. Winter, and I. Goldenfeld, Phys. Rev. B **38**, 12 937 (1988).
[14] A. Hoareau, P. Mélinon, B. Cabaud, D. Rayane, B. Tribollet, and M. Broyer, Chem. Phys. Lett. **143**, 602 (1988).
[15] D. Rayane, P. Melinon, B. Cabaud, A. Hoareau, B. Tribollet, and M. Broyer, J. Chem. Phys. **90**, 3295 (1989).
[16] B. Delley, J. Phys. C **17**, L551 (1984).

[17] T. T. Tsong, Surf. Sci. **177**, 593 (1986).
[18] W. A. Saunders, Phys. Rev. Lett. **62**, 1037 (1989).
[19] C. Baladrón, J. M. López, M. P. Iñiguzez, and J. A. Alonso, Z. Phys. D **11**, 323 (1989).
[20] F. Liu, M. R. Press, S. N. Khanna, and P. Jena, Phys. Rev. Lett. **59**, 2562 (1987).
[21] S. Sugano, A. Tamura, and Y. Ishii, Z. Phys. D **12**, 213 (1989).
[22] M. Nakamura, Y. Ishii, A. Tamura, and S. Sugano, Phys. Rev. A **42**, 2267 (1990).
[23] E. Lipparini and A. Vituri, Z. Phys. D **17**, 57 (1990).
[24] F. Garcias, J. A. Alonso, J. M. López, and M. Barranco, Phys. Rev. B **43**, 9459 (1991).
[25] R. N. Barnett, U. Landman, A. Nitzan, and G. Rajogopal, J. Chem. Phys. **94**, 608 (1991).
[26] W. Muller, Naturwissenschaften **29**, 33 (1941).
[27] A. Wagner and T. M. Hall, J. Vac. Sci. Technol. **16**, 1871 (1979).
[28] H. Helm and R. Möller, Rev. Sci. Instrum. **54**, 837 (1983).
[29] P. Joyes and J. van de Walle, J. Phys. (Paris) **47**, 821 (1986).
[30] H. Yamada and Y. Torii, Rev. Sci. Instrum. **57**, 1282 (1986).
[31] M. Watanabe, Y. Saito, S. Nishigaki, and T. Noda, Jpn. J. Appl. Phys. **27**, 344 (1988).
[32] Y. Saito, M. Minami, T. Ishida, and N. Noda, Z. Phys. D **11**, 87 (1989).
[33] J. Orloff and L. W. Swanson, J. Appl. Phys. **50**, 2494 (1979).
[34] G. A. Harrower, Rev. Sci. Instrum. **26**, 850 (1955).
[35] P. Fayet and L. Wöste, Z. Phys. D **3**, 177 (1986).
[36] S. Papadopoulos, D. L. Barr, and W. L. Brown, J. Phys. (Paris) **47**, NC2-101 (1986).
[37] W. A. Saunders and S. Fedrigo, Chem. Phys. Lett. **156**, 14 (1989).
[38] I. Halperin, Annu. Rev. Nucl. Sci. **9**, 245 (1959).
[39] J. Krauthamer, Ann. Phys. (N.Y.) **32**, 537 (1938); S. Norrman, T. Anderson, G. C. Granqvist, and O. Henderi, Phys. Rev. B **18**, 674 (1978); H. G. Craighead and G. A. Nilasson, Appl. Phys. Lett. **44**, 1134 (1984).
[40] N. Dam and W. Saunders, Z. Phys. D **19**, 85 (1991).
[41] Ph. Buffat and J. P. Borel, Phys. Rev. A **13**, 2287 (1976).
[42] Lord Rayleigh, *Theory of Sound* (Dover, New York, 1945), Vol. 2, p. 374.
[43] N. Bohr and J. A. Wheeler, Phys. Rev. **56**, 426 (1939).
[44] R. D. Present and J. K. Knipp, Phys. Rev. **57**, 751 (1940).
[45] W. J. Swiatecki, Phys. Rev. **104**, 993 (1956).
[46] R. C. Tolman, J. Chem. Phys. **175**, 333 (1949).
[47] W. A. Saunders, Phys. Rev. Lett. **64**, 3046 (1990).
[48] W. A. Saunders, Phys. Rev. Lett. **66**, 840 (1991).
[49] L. Wilets, *Theories of Nuclear Fission* (Oxford University, Oxford, 1964).
[50] W. A. Saunders and N. Dam, Z. Phys. D **20**, 111 (1991).
[51] P. Joyes and P. Sudraud, Surf. Sci. **156**, 451 (1985).
[52] C. Bréchignac, Ph. Cahuzac, F. Carlier, and M. de Frutos, Phys. Rev. Lett. **64**, 3046 (1990).
[53] S. Saito and M. L. Cohen, Phys. Rev. B **38**, 1123 (1988).

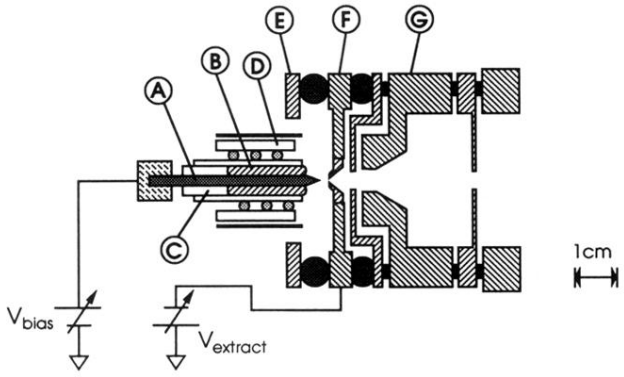

FIG. 1. The liquid-metal ion source (LMIS) used in present experiments. The labeled components are A, the etched tungsten needle; B, molten Au; C, ceramic plug and reservoir; D, heat shield; E, retaining ring; F, high-voltage extractor electrode; and G, asymmetric triode lens system. The connection of the source bias voltage (typically 250–300 V) and the extractor voltage (typically, −5 kV) are shown. Lens supply voltages are not indicated.

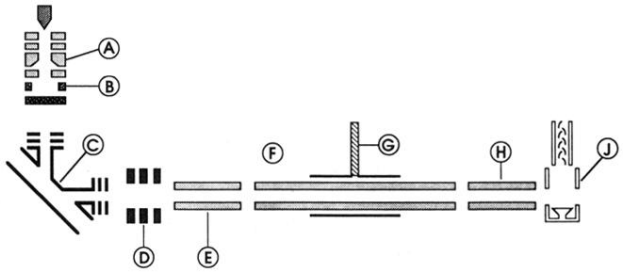

FIG. 2. The layout of the cluster source and the triple quadrupole mass spectrometer. The labeled components are A, the LMIS; B, beam deflectors; C, parallel-plate electrostatic energy filter with input and output trim lenses; E, Q1, F, Q2, G, gas inlet, and H, Q3; and J, the Daly conversion dynode and secondary electron multiplier. The lengths of Q1 and Q3 are 20 cm. Q2 has a length of 60 cm.